Optimized servo-speed control of wind turbine coupled to doubly fed induction generator

Abdelhamid Mansouri, Fateh Krim
Laboratory of Power Electronics and Industrial Control (LEPCI), Department of Electronics, Faculty of Technology,
University of Ferhat Abbas Setif 1, Maabouda, Algeria

Article Info

ABSTRACT

Optimal control of any variable speed wind turbine needs maximum power point tracking (MPPT) coupled to doubly fed induction generator (DFIG) for better power generation. This paper offers a novel direct power servo-speed control of wind turbine. This latter is based on DFIG optimal hysteresis MPPT inverter current control combined with space voltage modulation (SVM) inverter voltage technique, thus providing a stable and continuous energy flow to power grid. In this design, the asynchronous machine stator is directly connected to the grid. Bidirectional power converter, acting as frequency converter, is rotor circuit located. Rectifier supplies rotor windings with voltages and reference frequency resulting from control procedure of the power exchange between the stator and grid. Inverter is directly controlled by means of SVM technique to maintain direct current (DC) bus voltage constant. Simulation results show that the proposed configuration improves power converters efficiency due that rotor circuit needs less power than stator circuit which is injected into the grid.

Corresponding Author:

Fateh Krim
Department of Electronics, Faculty of Technology, University of Ferhat Abbas Setif 1
Maabouda City 19000, Algeria
Email: krim_f_ieee_org@yahoo.fr

1. INTRODUCTION

Global challenge is launched today by governments, industrials and researchers to face energy crises due to world population and consumption growth, poor infrastructure and unexplored different renewable energy sources. In this context, they are working together to make use of several cleaner power forms, mainly wind energies, solar sources to produce electricity, hydropower which provides electrical energy by water movement, geothermal energy to produce electricity using very hot water of aquifers in earth subsoil, without forgetting energy of biomass which provides energy through plant organic matter or animal origin. Among these sources, after hydropower, wind power is the most important, fastest growing configurations in wind turbine market, and first promising renewable energy source due to power electronics technology development, plants control and optimization in last three decades [1].

Recently, wind energy turbines have experienced strong growth in many regions, particularly in Europe and the United States due to manufacturing reduction costs [1]–[4]. However, this energy is very fluctuating due to the high variability of wind speed which could negatively affect voltage and current quality injected to the three-phase grid.

Conversion of wind energy into electrical energy can be done using various types of electrical machines. In this context, variable speed wind turbine based on doubly fed induction generator (DFIG) large power supply is the most used due to robustness, ease of maintenance and control improvement of energy

efficiency due to its rotational speed adapted to wind movements [1], [5]–[10]. But there is a constant trade-off between equipment capital costs and gains in efficiency.

Carlin *et al*. [11] prepared the history and state of the art of variable-speed wind turbine technology, on April 2003. In his published book, in 2021 [12], Okedu states that, since 2000, important improvements have been made by developments of wind energy technology. In Blaabjerg and Chen's research [13], due to the technological improvement of wind turbines from fixed speed to variable speed, DFIG has very attractive characteristics as a variable-speed wind turbine in the fast-growing market. The DFIG advantage is that the power electronic equipment based on two back-to-back pulse width modulation (PWM) power converters is only a fraction of the total power rating, that is, typically 20 to 30%. Therefore, its size, cost, and losses are much smaller compared to a full-size power converter. El-Sattar *et al*. [14] performed an analysis of DFIG variable speed wind turbine, taking into account different power converter capacities with 20%, 25% and 30% of the rated power. Therefore, the losses in the converter are lower compared to a system where the converter has to handle the full power leading to an improvement in the total efficiency. But, the DFIG system is found more stable for the 30% for the power converter capacity under network disturbance. Erlich *et al*. [15] proves that lower inverter rating results in lower losses and thus higher overall efficiency, and lower costs without grid faults effects on DFIG. In study [7], the losses are shown separately for the generator and for the insulated gate bipolar transistor (IGBT) inverters. Approximately 2% to 3% efficiency improvement reducing cost of DFIG SVM control can be obtained, compared to direct line adjustable speed generator, for rated power above 1.5 MW.

This paper offers a suitable space voltage modulation (SVM) combined with hysteresis maximum power point tracking (MPPT) servo-speed control showing improvement of voltage quality in term of harmonics content leading to better inverter efficiency. Comparatively to the previous works, the control power used is minimal compared to nominal DFIG power. This paper contains four sections as follows: after an introduction, in section 2, we present research method: DFIG based wind turbine energy conversion, chain control structure, DFIG dynamics modeling will be detailed. An overview of rotor side hysteresis MPPT control will be provided. Simulation results will be presented and discussed in section 3, to conclude the paper in section 4.

2. RESEARCH METHOD

It is important to apply the best control strategy of variable speed wind turbine for DFIG based wind energy conversion to regulate electromagnetic torque adjusting the mechanical speed for better power generation. Objective of this paper is to offer a novel direct power servo-speed control of wind turbine. This latter is based on DFIG optimal hysteresis MPPT inverter current control combined with SVM inverter voltage technique. This implementation provides stable and continuous power to three-phase electrical grid through direct current (DC)-link voltage, resistance-inductance (RL) filter and step-up transformer.

2.1. DFIG based wind turbine energy conversion

DFIG configuration variable speed wind turbine based on two controls systems; rotor side converter (RSC) and grid side converter (GSC), is shown in Figure 1. Chain consists of turbine, an adjusting rotating speed gearbox, DFIG power supply and two back-to-back PWM power converters linked by DC voltage stage connected to three-phase electrical grid through RL filter and three-phase step up transformer, where voltage levels are adjusted to match with grid.

In this design, double power supply refers to machine stator voltage connected directly to electrical grid and to rotor voltage supplied by two cascaded converters [16], [17]. Two variable frequency power converters, sized for generator nominal power fraction, are located in rotor circuit. Insertion of converters between rotor and grid feeds rotor windings with set point voltages and frequency received from control procedure of power exchange between stator and grid, to ensure transfer rotor power by controlling DC bus voltage keeping its level constant providing proper inverter working. Smoothing inductors inserted at inverter terminals allow significant current harmonics reduction. Despite presence of sliding contacts reducing slightly robustness in disturbance cases, majority of wind projects use asynchronous generator driven by rotor. This configuration presents an economical advantage with respect to power converters because power transmitted through rotor circuit is smaller than stator power [5]–[7].

2.2. Energy conversion chain control structure

Wind turbine drives DFIG at variable rotating speed through gearbox. DFIG stator is connected through a transformer to the electrical grid. Rotor is grid connected through three-phase current filter and two bidirectional static converters PWM control, cascaded across DC bus voltage [18], [19]. Major advantage of this wind power system lies in ensuring two voltage controls operation: i) inverter DFIG-RSC of regulated stator active and absorbed reactive powers and torque, ii) rectifier GSC supplies rotor windings with voltages and

reference frequency received from control procedure of the power exchange between the stator and grid, and iii) inverter is directly controlled to keep fixed DC bus voltage.

2.3. DFIG Dynamics modeling

Wind turbine coupled to DFIG in Figure 2, is fitted with blades of length R fixed to pitch angle β, running under wind speed v_w, providing wind kinetic power [20] P_w in (1):

$$P_w = \frac{1}{2}\rho\pi R^2 v_w^3 \tag{1}$$

where ρ: Air density, Pw is converted to shaft mechanical power, driving DFIG through speed gain G gearbox to produce electricity.
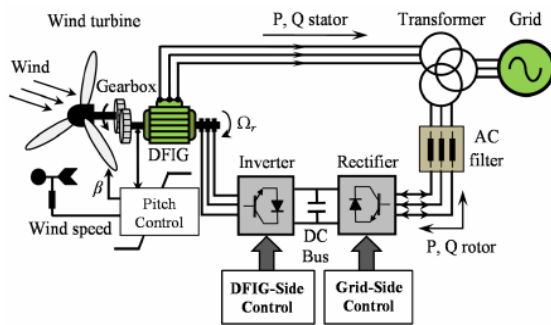

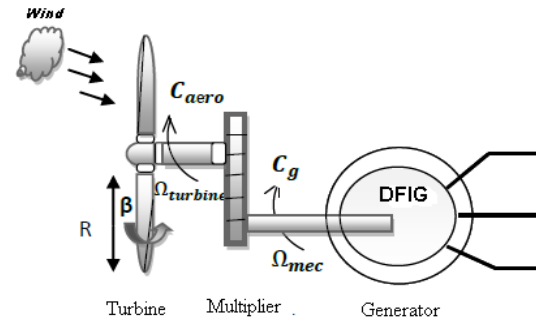Figure 1. DFIG configuration variable speed wind turbine

Figure 2. Wind turbine coupled to DFIG

Turbine mechanical power P_{Turb} extracted by wind speed is linked to P_w by power coefficient C_p [5]–[7]:

$$P_{Turb} = C_p . P_w \tag{2}$$

Aerodynamic power coefficient C_p, differs for each wind turbine having different blade lengths, depending on blades pitch angle β_i and specific speed λ defined as ratio of blade tip speed ($\Omega_{Turb}. R$=peripheral tangential speed) and wind speed v_w. Ω_{Turb}: Turbine angular rotating speed. Power coefficient $C_p(\lambda, \beta_i)$ is often derived from practical measurements and expresses turbine efficiency to transform wind kinetic energy into mechanical energy. Whereas turbine mechanical power is (3):

$$P_{Turb} = \frac{1}{2}C_p(\lambda, \beta_i)\rho\pi R^2 v_w^3 \tag{3}$$

From particular 1.5 MW rated power wind turbine study, we deduce nonlinear empirical function of speed ratio λ for different blades pitch angles β_i [5]:

$$C_p(\lambda, \beta_i) = (0.44 - 0.0167\beta_i)sin(\pi \frac{\lambda-3}{15-0.3\beta_i}) - 0.00184(\lambda - 3)\beta_i \tag{4}$$

Figure 3 shows power characteristic curves of power coefficient $C_p (\lambda, \beta_i)$ expressed by (4). For a constant angle β_i (i = 1, 2, 3, 4, 5), we could keep speed ratio λ constant and equal to optimal value λ_{opt} at each instant, power captured by wind turbine would be maximum P_{opt}. This condition can only be verified with use of variable speed wind turbines, by exploiting characteristic curves maxima, which will be studied in the section 2.5.

2.3.1. DFIG model

DFIG model in d-q rotating reference frame is developed using Park's transform for better dynamic behavior for: stator rotor voltages, electromagnetic torque and principle of constant stator flux and rotor current I_{rq} control of DFIG oriented on Park frame axis [21]. Stator voltage frequency being imposed by electrical grid, rotor currents pulsation ω_r is given by (5):

$$\omega_r = \omega_s - p.\Omega \qquad (5)$$

where ω_s is stator currents pulsation in (rad/s); Ω is DFIG rotating speed; p is pole pairs number. Stator and rotor angles θ_s and θ_r are obtained respectively by integration of ω_s and ω_r.
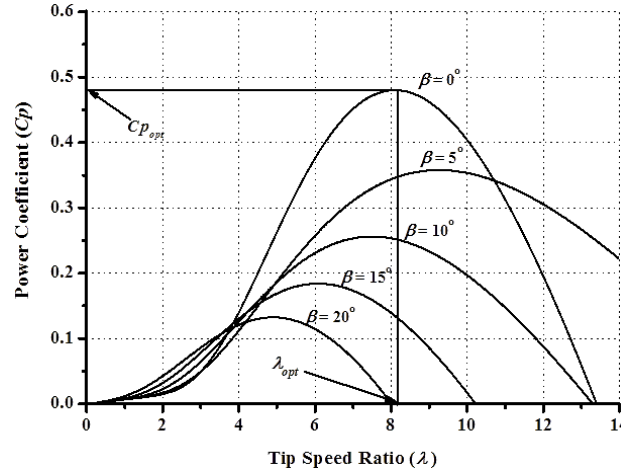

Figure 3. Influence of pitch angle on power coefficient

2.3.2. DC bus regulation
DC bus electrical circuit is shown in Figure 4. Using Kirchhoff law, we establish in (6) and (7):

$$\frac{dV_{dc}(t)}{dt} = \frac{1}{C} i_{dc}(t) \, ; \qquad (6)$$

$$i_{dc} = i_1 - i_2 \qquad (7)$$

where i_1 is rectified current, i_2 is current to invert, i_{dc} is capacitor load current. DC bus voltage is obtained from current i_{dc} integration of relation (6) flowing in capacitor C to have rectified V_{dc}.

$$V_{dc} = \frac{1}{C} \int_{t_1}^{t_2} i_{dc} \, dt + V_{dc0} \qquad (8)$$

$V_{dc0} = 0 \ V$: initial voltage value.

Given DFIG power supplied fluctuations, DC bus voltage adjustment is required via regulation loop with conventional integral proportional IP corrector, unlike PI regulator; having advantage of not generating additional zeros in closed loop transfer function (CLTF) (a slow zero could decrease system dynamic performance) [22], [23]. DC link capacitor smooth DC voltage fluctuations and strengthen DC bus. This is important because any DC bus voltage ripple shows up as phase currents ripple, leading to torque ripple. Ultimately, we should have specification for DC bus maximum allowable voltage ripple under worst case conditions. Usually, this number ranges from 1 to 10%. It depends on maximum allowable torque ripple.

2.4. Rotor side MPPT optimized direct control
Optimum power characteristic curves of wind turbine are strongly nonlinear and bell-shaped as shown in power-speed plane of Figure 5. For each wind speed v_i, system must extract maximum power P_{opt} described by nonlinear (9) to find optimum rotating speed Ω_{opt} [5]:

$$P_{opt} = \frac{1}{2} C_p^{opt}(\lambda_{opt})\rho S v_w^3 \qquad (9)$$

Wind power system ideal operation requires Figure 5 curve perfect tracking. To approach this goal, specific control strategy called maximum power point tracking MPPT corresponding to zone II must be used [24]. This strategy is to control electromagnetic torque to adjust turbine mechanical rotational speed for better power generation as explained in paragraphs here down.
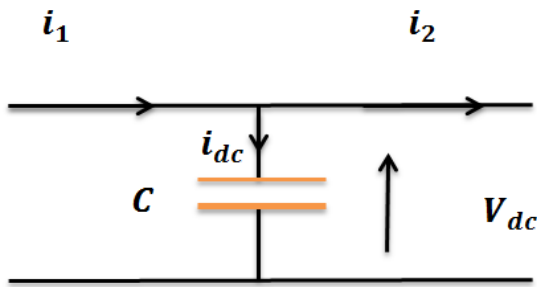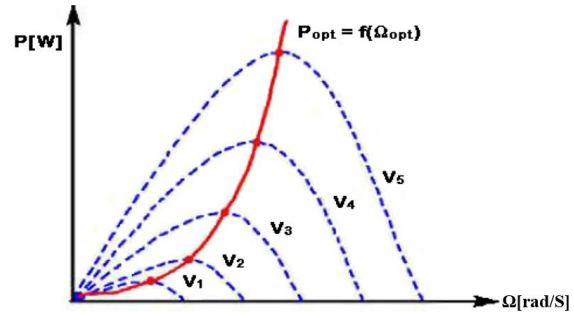
Figure 4. DC bus electrical circuit

Figure 5. Wind turbine characteristics in power-angular speed plane

2.4.1. Direct power servo-speed control

Technique without speed control is an open loop device. To improve dynamics response, direct power servo-speed control consists of using conventional proportional integral PI type regulator. This control strategy involves controlling electromagnetic torque on turbine shaft in order to adjust mechanical speed to maximize electrical power.

Wind fluctuating nature causes disturbances in wind energy conversion system and creates continuous power variations. Therefore, this strategy assumes that machine electromagnetic torque equals its reference T_{em-ref} regardless power. This is achieved by using adequate servo-speed to have reference electromagnetic torque in (10):

$$T_{em-ref} = C_{ass}(\Omega_{ref} - \Omega_{mec}) \tag{10}$$

C_{ass} is PI speed regulator. Ω_{ref} is Reference rotating speed. Ω_{ref} depends on turbine speed $\Omega_{Turb\text{-}ref}$ to be set in order to maximize extracted power:

$$\Omega_{ref} = G.\Omega_{Turb-ref} \tag{11}$$

$\Omega_{Turb\text{-}ref}$ corresponds to optimum value of specific speed λ_{opt}. Maximum power coefficient $C_{p\text{-}max}$ can be deduced from speeds ratio defining specific speed λ_{opt}:

$$\Omega_{Turb-ref} = \frac{\lambda_{opt}V_w}{R} \tag{12}$$

DFIG servo-speed horizontal axis wind turbine MPPT closed loop control block diagram is shown in Figure 6, having inputs: blades pitch angle β, wind speed V_w and electromagnetic torque T_{em} supplied by generator:

2.4.2. SVM inverter voltage control

SVM control is different from all conventional modulation techniques in that the control signals are established taking into account the states of the three inverter arms at the same time. It consists in reconstructing the desired reference voltage vector from eight voltage vectors, during a modulation period by a sequence of adjacent zero vectors corresponding to the possible states of this 6 switches inverter. SVM is the most suitable modulation technique for variable speed drive applications of AC electrical machines via the three-phase inverter [25]. Unlike others methods, SVM relies on a digital algorithm to determine switching sequences for an output voltage vector that approaches the reference vector. The symmetry distribution of the conducting duration reduces the total harmonic distortion (THD). SVM is sophisticated because it eliminates the need for harmonic elimination filters.

2.4.3. Hysteresis inverter current control

Simplest implementation and quick response hysteresis control strategy imposes inverter insulated gate bipolar transistor IGBT switching to maintain measured phase current within fixed hysteresis band around reference current in Figure 7. Limits of switching band can be fixed type: fixed band hysteresis switching (FBHC) for choppers or sinusoidal band hysteresis switching (SBHC) for inverters, [26], [27]. Therefore, three static inverter switching conditions are defined in terms of logic states as follows:

I_i $(i = $ a, b, c) is actual stator phase currents (I_a, I_b, I_c), I_{iref} is reference currents from three arms inverter control circuits, h is chosen hysteresis band not to exceed permissible semiconductors switching frequency control to sufficiently minimize current harmonics. Hysteresis inverter action described in Figure 7 produces triangular pulse train current error waveform, and inverter output U_o, U_{dc} being the inverter input.
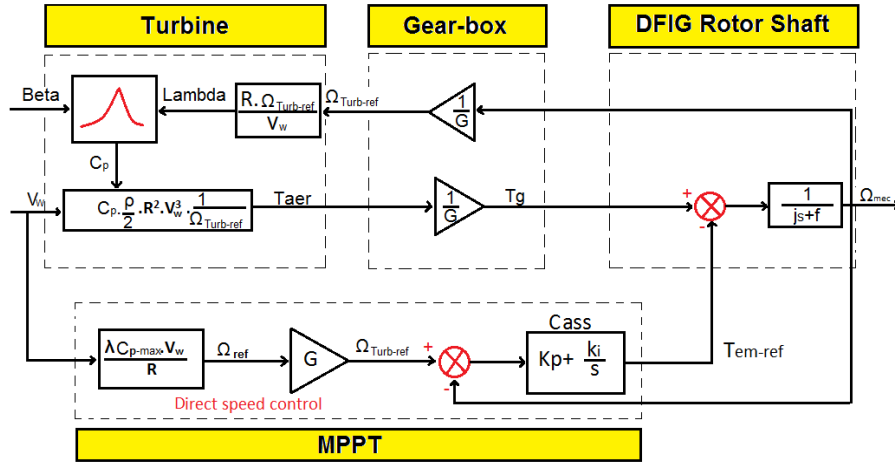

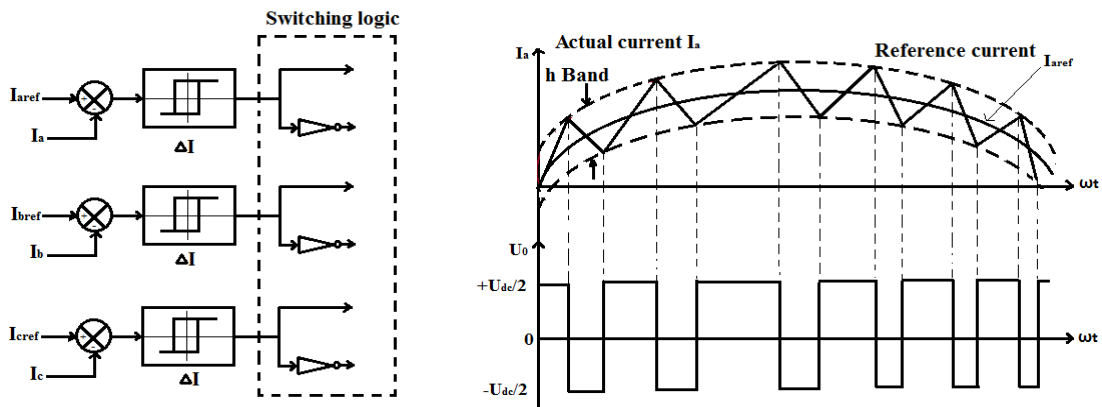Figure 6. Block diagram of direct servo-speed control

Figure 7. Hysteresis inverter current control block diagram

3. RESULTS AND DISCUSSION
3.1. DFIG simulation results and discussion

Horizontal axis three blades wind turbine and DFIG parameters are given in Table 1. Simulation results are obtained for critical case of smooth step wind speed profile v_w varying from 8 to 12 m/s at 0.2 s of Figure 8(a). Specific speed lambda λ in Figure 8(b), power coefficient C_p in Figure 8(c), DFIG rotating speeds and DFIG electromagnetic torque $T_{em-DFIG}$ in Figures 8(d) and 8(e), DC link voltage without inverter in Figure 8(f). DFIG stator and rotor voltages and currents are represented in Figures 9(a), 9(b), 10(a), 10(b), 11(a), and 11(b).

In Figure 8(b) lambda reaches its optimal value 18.5 after 0.04 s. An attenuation of 6 units at 0.2 s is due to turbine and generator assembly inertia, to reach again its maximum 18.5 after 0.03 s. C_p of Figure 8(c) reaches quickly its maximum 0.528, but decreases to 0.02 rapidly thereafter 0.178 s, to reach 0.45, smaller than previous value, to decrease again to value 0.018 and remain constant until 1.6 s. In Figure 8(d), at 0.2 s we notice respectively an increase 9.2 to 13.9, 40.55 to 61.1 and 81.5 to 122.2 rad/s speed variations well adapted to wind speed profile. Figure 8(e) shows $T_{em-DFIG}$ variation proportional to w_{m-DFIG}. At 0.2 s, we notice an increase 9.4 to 21.4 Nm tracking wind speed. $T_{em-DFIG}$ variation is well adapted to wind speed changing. Figure 8(f) shows DC bus voltage Vdc without inverter proportional to wind speed increase. From 80 V at 0.2 s, Vdc increase again to 420 V until 1.6 s, leading to instability.

Table 1. Wind turbine and DFIG parameters

| Wind turbine parameters		DFIG Parameters	
Nominal power	$P_N = 1.5\ MW$	Nominal power	$P_N = 7.5\ kW$
Air density	$\rho = 1.22\ Kg/m^3$	Nominal Voltage	$U_N = 220/380\ V$
Inertia angular moment	$J = 2\ kg.m^2$	Rated rotational speed	$N_n = 1440\ rpm$
Friction factor	$f = 0.061\ Nm.s/rad$	Pole pairs number	$p = 2$
Pitch angle	$\beta = 1°$	Rotor and stator leakage inductances	$L_r = L_s = 10\ mH$
Optimal specific speed	$\lambda = 18.78$	Stator resistance	$R_S = 1.63\ m\Omega$
Maximum power factor	$C_{pmax} = 0.49$	Rotor resistance	$R_r = 1.93\ m\Omega$
Wind rotor radius	$R = 16\ m$	Mutual inductance	$L_m = 2\ mH$
Multiplier gain	$G = 4.4$	Short circuit current	$Isc = 8.21\ A$
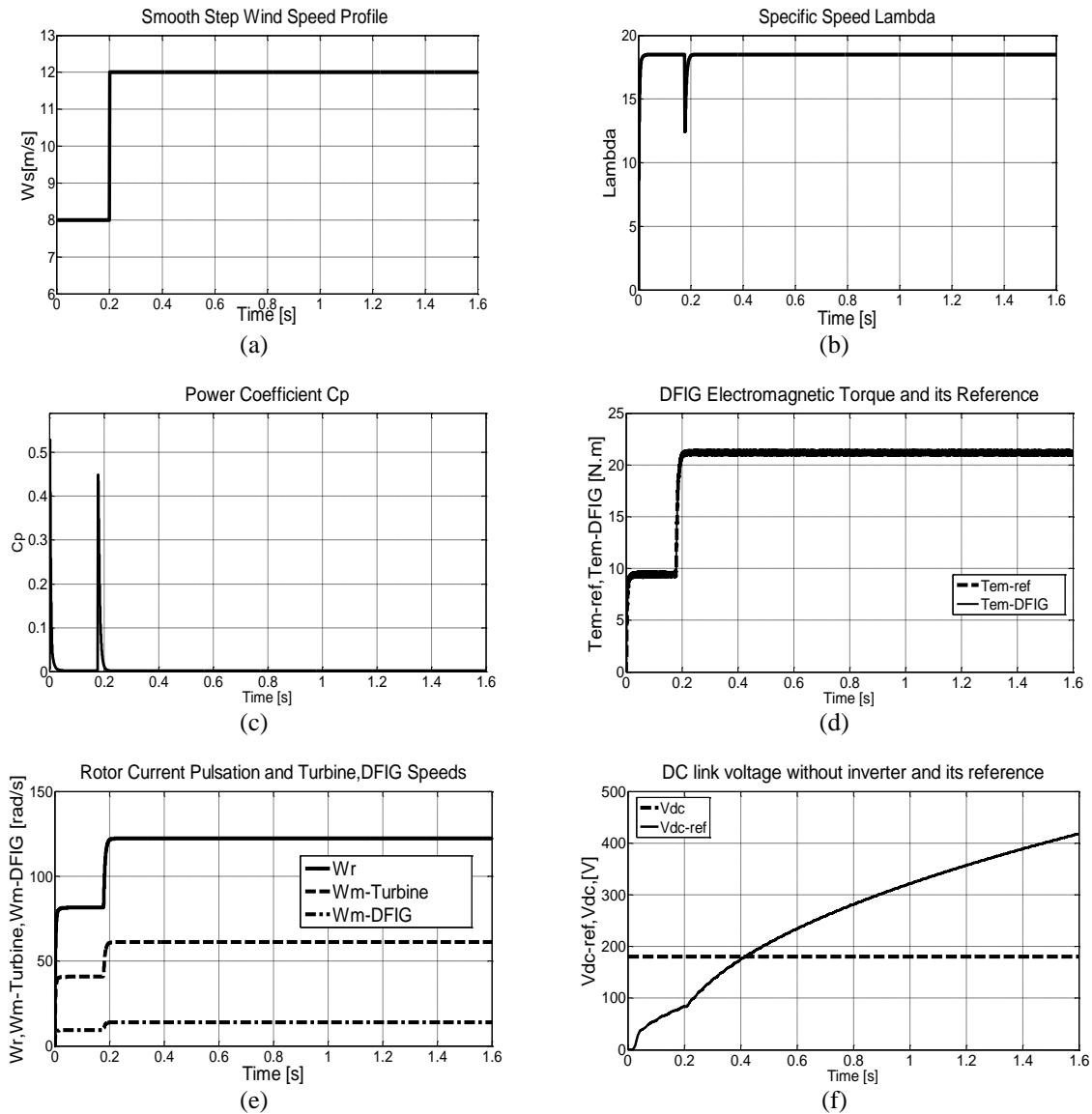
Figure 8. Simulation results regarding the DFIG performance for a step wind speed change in, (a) smooth step wind speed profile, (b) specific speed lambda, (c) power coefficient, (d) DFIG rotating speeds, (e) DFIG Electromagnetic torque and its reference, and (f) DC link voltage without inverter

In Figures 9(a) and 9(b), from 0.2 s, we notice an increase 80 - 122.2 V (peak). DFIG stator three-phase voltage variation is well adapted to wind speed changing. In Figures 10(a) and 10(b), from 0.2 s, steady states DFIG rotor voltage of 60 V is reached. In Figures 11(a) and 11(b), at 0.2 s, an increase 2.6 to 6 A. Generator currents variation is well adapted to wind speed changing.
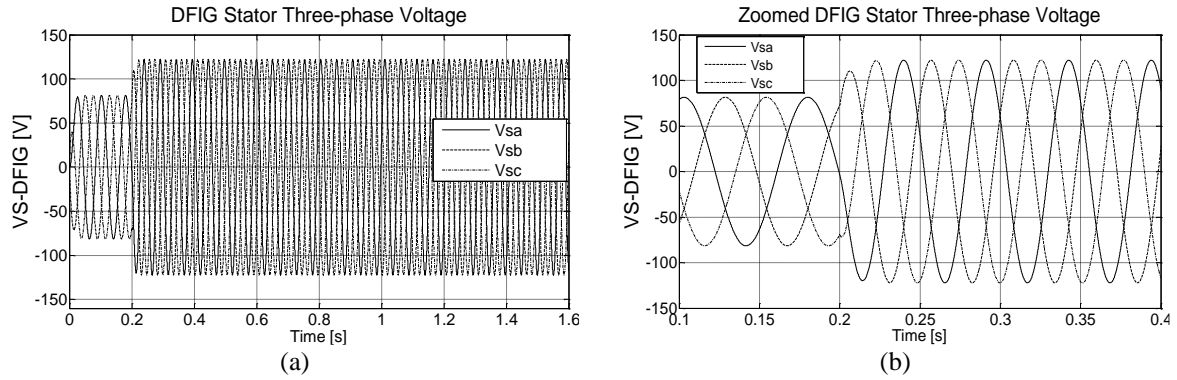
Figure 9. Simulation results for DFIG stator voltage in, (a) three-phase voltage and, (b) Zoom of (a) (0.1 to 0.4 s)

3.2. Grid side control and results discussion

In order to exchange controlled power, coupling wind power plant to grid must comply with the following constraints: frequency, amplitude and phase; synchronized by using phase-lock loop (PLL). Global wind energy production chain is connected to balanced voltage three-phase grid via PWM inverter and three-phase filter. Inverter role on GSC is to keep DC bus voltage constant whatever power magnitude and direction, generating loading current necessary for capacitor, particularly in starting phase by currents control transmitted to grid through RL filter. Inverter is controlled so as to impose references to phase-to-neutral voltages from DC bus voltage measurement, according to conventional closed loop grid link control [28]. Knowing that DFIG must supply or absorb power at unity factor for GSC, $I_{q\text{-ref}} = 0$ A. Knowing that DFIG must neglect magnetizing current only from stator, $I_{d\text{-ref}} = 0$ A. DC voltage reference is regulated to nominal value V_{dc}. Rotor reference speed Ωref is determined according to MPPT energy extraction. The details of the methodology used are given below.
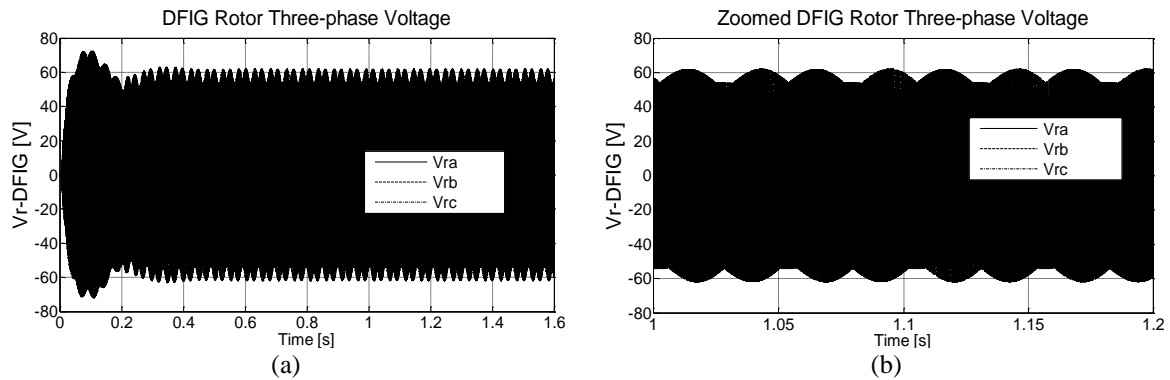

Figure 10. Simulation results for DFIG rotor voltage in, (a) three-phase voltage and (b) zoom of (a) (0.1 to 0.4 s)
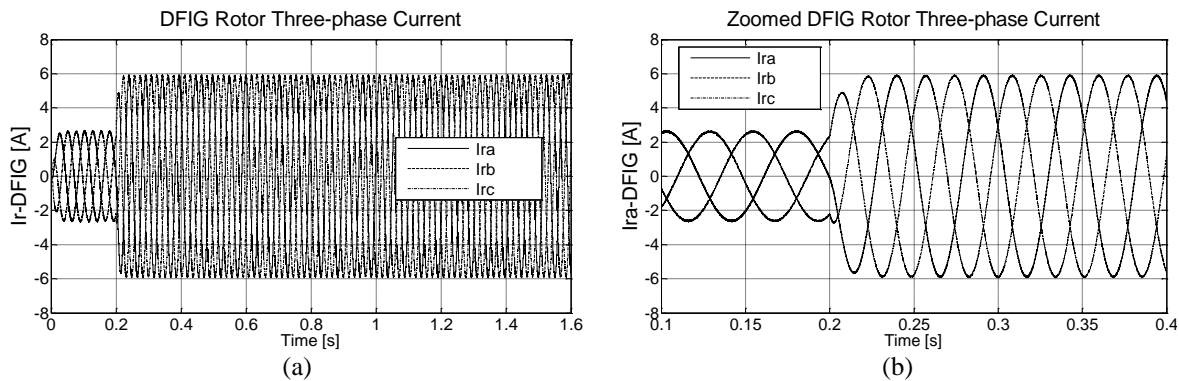

Figure 11. Simulation results for DFIG stator current in, (a) three-phase current and (b) zoom of (a) (0.1 to 0.4 s)

3.2.1. Grid side currents control

Direct I_{sd}, and quadratic currents I_{sq} controlled were obtained from grid link model inversion by Park's transform. It includes three specific actions:

— Transformer secondary voltage compensation:

$$\begin{cases} e_{q\_est} = L_t.\omega_s.i_{tq} \\ e_{d\_est} = L_t.\omega_s.i_{td} \end{cases} \tag{13}$$

— Decoupling d and q axis action:

$$\begin{cases} U_{md\_reg} = U_{bd_{ref}} - e_{q\_est} + U_{pd\_mes} \\ U_{mq\_reg} = U_{bd_{ref}} - e_{d\_est} + U_{pq\_mes} \end{cases} \tag{14}$$

— Closed loop currents control using C_i regulator:

$$\begin{cases} U_{bd\_ref} = C_i.(i_{td_{ref}} - i_{td_{mes}}) \\ U_{bq\_ref} = C_i.(i_{tq_{ref}} - i_{tq_{mes}}) \end{cases} \tag{15}$$

3.2.2. Power regulation

Regulated active and reactive powers controlled are given by Park's model leading to relations (16):

$$P = v_{pd}.i_{td} + v_{pq}.i_{td}$$
$$Q = v_{pq}.i_{td} - v_{pd}.i_{tq} \tag{16}$$

By inverting relations (16), it is then possible to impose direct and quadratic reference currents (17) for active and reactive powers:

$$\begin{cases} i_{td-ref} = \frac{P_{ref}.v_{pd-mes} + Q_{ref}.v_{pq-mes}}{v_{pd-mes}^2 + v_{pq-mes}^2} \\ i_{tq-ref} = \frac{P_{ref}.v_{pq-mes} + Q_{ref}.v_{pd-mes}}{v_{pd-mes}^2 + v_{pq-mes}^2} \end{cases} \tag{17}$$

3.2.3. Power transits control to grid

Power stored in capacitor and therefore DC bus voltages are controlled. By neglecting inverter and filter capacitor losses compared to power transmitted to grid, we need available power supplied by rectifier. If we neglect inverter loss, therefore RSC power:

$$P_{dc\_mac} = u.i_{m\_mac} \tag{18}$$

Power stored in capacitor dissipated in DC bus, is noted $P_{loss-condens}$. Rest of power is expressed by (19):

$$P_{dc-rec-ref} = P_{dc\_mac} - P_{condens-ref} - P_{loss-condens} \tag{19}$$

It is therefore possible to impose necessary capacitive current by adjusting power transits to grid.

Regarding the servo-speed, for the same smooth-scale wind speed profile, see Figure 8(a), we observe the controlled DFIG active P, see Figure12(a), reactive power Q, see Figure12(b), quadratic axis current iq, see Figure 12(c), direct axis current id, see Figure 12(d), DC link voltage over 1.6 s period, see Figure 12(e), inverter three-phase currents, see Figures 13(a), 13(b)) and inverter voltages, see Figures 14(a), 14(b). Controlled active P and reactive Q powers are shown respectively in Figures 12(b) and 12(c): P is superposed to its reference P_{ref}. It starts increasing with a peak of 240 W at t_p=0.2 s to reach a low steady state value of 100 W. This shows that the control power used is minimal compared to that of the nominal DFIG: $P = 100\ W/Pn = 7500\ W = 1.33\%$. Q oscillates around its reference set to average $Q_{ref} = 0$ VAR for unity PF to optimize the generated energy. In Figures 12(d) and 12(e), DFIG direct I_d and quadratic I_q currents: I_d is superposed to its reference. Start increasing at 0.2 s with a peak of 5 A to reach steady states value of 2 A. At start-up, current I_q reaches transient state value of 4 A to return to zero as Q. DC bus voltage regulation is shown in Figure 12(e) with an overshoot of 11.2% at $t_p = 0.91$ s. The bus reaches its reference value V_{dc-ref}=180 V, settling time t_s=260 ms, with low oscillations superposed on its reference voltage.
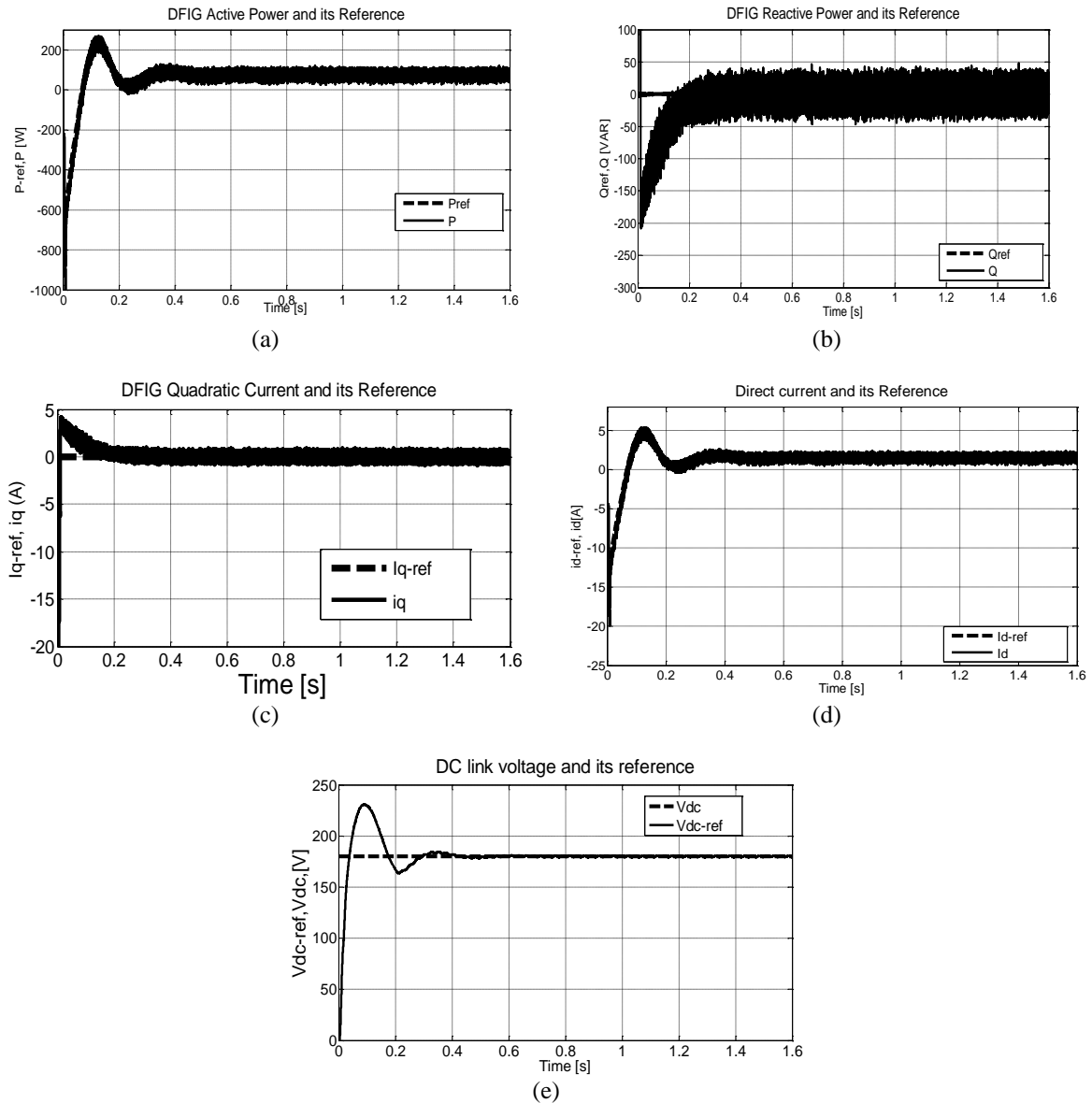
Figure 12. Simulation results for DFIG and DC link in; (a) active power and its reference, (b) reactive power and its reference, (c) direct current and its reference (d) quadratic current and its reference, and (e) DC link voltage and its reference
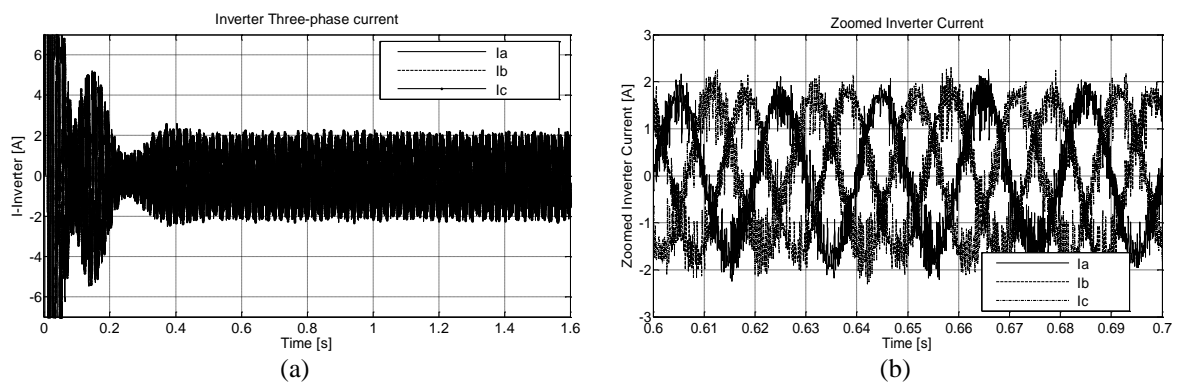

Figure 13. Simulation results for inverter current in; (a) three-phase current and (b) zoom of "a" (0.6 to 0.7 s)

Figures 13(a) and 13(b) show inverter three-phase current I-inverter. I-inverter increases after 0.2 s, to reach steady states value of 2 A; showing current harmonic distortion. Unlike, three-phase voltage V-inverter showed in Figures 14(a) and 14(b) remain constant at maximum value of 50 V despite wind speed changing.
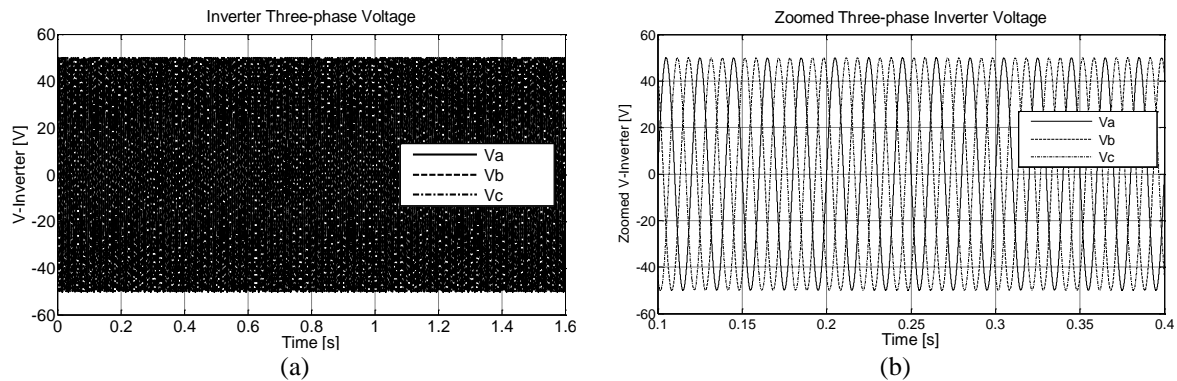

Figure 14. Simulation results for inverter voltage: (a) three-phase voltage and (b) zoom of "a" (0.1 to 0.2 s)

4. CONCLUSION

From DFIG and grid side control results, servo-speed direct control is more efficient in static and dynamic states tracking leading to wind turbine efficiency, compared to indirect MPPT speed control. DFIG rotor current is flexibly controlled, reducing mechanical stress with low power consumption compared to DFIG rated value. This work may be a good basis for building practical DFIG wind turbine small-scale bench. Improvement of power electronics designs and costs reduction of manufacture, the balance may tilt in the favor of DFIG variable speed wind turbine. This technology could come to dominate the future of wind energy technology.

ACKNOWLEDGEMENTS

REFERENCES

[1] F. Blaabjerg and K. Ma, "Wind energy systems," *Proceedings of the IEEE*, vol. 105, no. 11, pp. 2116–2131, Nov. 2017, doi: 10.1109/JPROC.2017.2695485.
[2] A. D. Hansen, F. Iov, F. Blaabjerg, and L. H. Hansen, "Review of contemporary wind turbine concepts and their market penetration," *Wind Engineering*, vol. 28, no. 3, pp. 247–263, May 2004, doi: 10.1260/0309524041590099.
[3] M. Liserre, R. Cardenas, M. Molinas, and J. Rodriguez, "Overview of multi-MW wind turbines and wind parks," *IEEE Transactions on Industrial Electronics*, vol. 58, no. 4, pp. 1081–1095, Apr. 2011, doi: 10.1109/TIE.2010.2103910.
[4] P. Tchakoua, R. Wamkeue, M. Ouhrouche, F. Slaoui-Hasnaoui, T. Tameghe, and G. Ekemb, "Wind turbine condition monitoring: State-of-the-Art review, new trends, and future challenges," *Energies*, vol. 7, no. 4, pp. 2595–2630, Apr. 2014, doi: 10.3390/en7042595.
[5] R. Pena, J. C. Clare, and G. M. Asher, "Doubly fed induction generator using back-to-back PWM converters and its application to variable-speed wind-energy generation," *IEE Proceedings - Electric Power Applications*, vol. 143, no. 3, pp. 231–241, 1996, doi: 10.1049/ip-epa:19960288.
[6] A. Tapia, G. Tapia, J. X. Ostolaza, and J. R. Saenz, "Modeling and control of a wind turbine driven doubly fed induction generator," *IEEE Transactions on Energy Conversion*, vol. 18, no. 2, pp. 194–204, Jun. 2003, doi: 10.1109/TEC.2003.811727.
[7] S. Muller, M. Deicke, and R. W. De Doncker, "Doubly fed induction generator systems for wind turbines," *IEEE Industry Applications Magazine*, vol. 8, no. 3, pp. 26–33, 2002, doi: 10.1109/2943.999610.
[8] H. T. Jadhav and R. Roy, "A comprehensive review on the grid integration of doubly fed induction generator," *International Journal of Electrical Power & Energy Systems*, vol. 49, no. 1, pp. 8–18, Jul. 2013, doi: 10.1016/j.ijepes.2012.11.020.
[9] B. C. Babu and K. B. Mohanty, "Doubly-fed induction generator for variable speed wind energy conversion systems- modeling & simulation," *International Journal of Computer and Electrical Engineering*, vol. 2, no. 1, pp. 141–147, 2010, doi: 10.7763/IJCEE.2010.V2.127.
[10] H. Hachemi, A. Allali, and B. Belkacem, "Control of the powerquality for a DFIG powered by multilevel inverters," *International Journal of Electrical and Computer Engineering (IJECE)*, vol. 10, no. 5, pp. 4592–4603, Oct. 2020, doi: 10.11591/ijece.v10i5.pp4592-4603.
[11] P. W. Carlin, A. S. Laxson, and E. B. Muljadi, "The history and state of the Art of variable-speed wind turbine technology," *Wind Energy*, vol. 6, no. 2, pp. 129–159, Apr. 2003, doi: 10.1002/we.77.

[12] K. Okedu, "Transient analysis of variable- and fixed-speed wind turbines," in *Onshore Wind Farms*, AIP Publishing, 2021, pp. 1–18.

[13] F. Blaabjerg and Z. Chen, "Power electronics as an enabling technology for renewable energy integration," *The Korean Institute of Power Electronics*, vol. 3, no. 2, pp. 81–89, 2003.

[14] A. A. El-Sattar, N. H. Saad, and M. Z. S. El-Dein, "Dynamic response of doubly fed induction generator variable speed wind turbine under fault," *Electric Power Systems Research*, vol. 78, no. 7, pp. 1240–1246, Jul. 2008, doi: 10.1016/j.epsr.2007.10.005.

[15] I. Erlich, H. Wrede, and C. Feltes, "Dynamic behaviour of DFIG-based wind turbines during grid faults," *IEEJ Transactions on Industry Applications*, vol. 128, no. 4, pp. 396–401, 2008, doi: 10.1541/ieejias.128.396.

[16] K. Okedu, "Impact of power converter size on variable speed wind turbines," in *Onshore Wind Farms*, AIP Publishing, 2021, pp. 7–8.

[17] Alhato and Bouallègue, "Direct power control optimization for doubly fed induction generator based wind turbine systems," *Mathematical and Computational Applications*, vol. 24, no. 3, pp. 1–28, Aug. 2019, doi: 10.3390/mca24030077.

[18] A. Petersson, "Analysis, modeling and control of doubly-fed induction generators for wind turbines," Chalmers Univ. of Technology, Goteborg, Sweden, 2005.

[19] Z. Wang, G.-J. Li, Y. Sun, and B. T. Ooi, "Effect of erroneous position measurements in vector-controlled doubly fed induction generator," *IEEE Transactions on Energy Conversion*, vol. 25, no. 1, pp. 59–69, Mar. 2010, doi: 10.1109/TEC.2009.2037216.

[20] H. Polinder, F. F. A. Van Der Pijl, G.-J. De Vilder, and P. J. Tavner, "Comparison of direct-drive and geared generator concepts for wind turbines," *IEEE Transactions on Energy Conversion*, vol. 21, no. 3, pp. 725–733, Sep. 2006, doi: 10.1109/TEC.2006.875476.

[21] E. Rezaei, A. Tabesh, and M. Ebrahimi, "Dynamic model and control of DFIG wind energy systems based on power transfer matrix," *IEEE Transactions on Power Delivery*, vol. 27, no. 3, pp. 1485–1493, Jul. 2012, doi: 10.1109/TPWRD.2012.2195685.

[22] P. Verdelho and G. D. Marques, "DC voltage control and stability analysis of PWM-voltage-type reversible rectifiers," *IEEE Transactions on Industrial Electronics*, vol. 45, no. 2, pp. 263–273, Apr. 1998, doi: 10.1109/41.681225.

[23] A. Chaoui, J.-P. Gaubert, F. Krim, and L. Rambault, "IP controlled three-phase shunt active power filter for power improvement quality," in *IECON 2006 - 32nd Annual Conference on IEEE Industrial Electronics*, Nov. 2006, pp. 2384–2389, doi: 10.1109/IECON.2006.348043.

[24] X. Zhang, Y. K. Chen, and R. K. Calay, "Modelling and analysis of a novel wind turbine structure," *International Journal of Modelling, Identification and Control*, vol. 19, no. 2, pp. 142–149, 2013, doi: 10.1504/IJMIC.2013.054318.

[25] M. Z. Sujod, I. Erlich, and S. Engelhardt, "Improving the reactive power capability of the DFIG-based wind turbine during operation around the synchronous speed," *IEEE Transactions on Energy Conversion*, vol. 28, no. 3, pp. 736–745, Sep. 2013, doi: 10.1109/TEC.2013.2272975.

[26] M. Mohseni, S. M. Islam, and M. A. S. Masoum, "Enhanced hysteresis-based current regulators in vector control of DFIG wind turbines," *IEEE Transactions on Power Electronics*, vol. 26, no. 1, pp. 223–234, Jan. 2011, doi: 10.1109/TPEL.2010.2058816.

[27] A. Dwivedi and A. N. Tiwari, "Analysis of three-phase PWM rectifiers using hysteresis current control techniques: a survey," *International Journal of Power Electronics*, vol. 8, no. 4, pp. 349–377, 2017, doi: 10.1504/IJPELEC.2017.10005639.

[28] D. Xu, F. Blaabjerg, W. Chen, and N. Zhu, "Control of DFIG power converters," in *Advanced Control of Doubly Fed Induction Generator for Wind Power Systems*, Hoboken, NJ, USA: John Wiley & Sons, Inc., 2018, pp. 99–138.

BIOGRAPHIES OF AUTHORS

Fateh Krim received B.Sc. degree from Claude Bernard University of Lyon, France, in 1976, M. Sc and Engineer degrees in electrical engineering from Ecole Centrale, Lyon, in 1979, the PhD from Polytechnic National Institute of Grenoble, France, and the special doctorate from University of Sétif, Algeria, in 1982 and 1996 respectively. He was head of IC design department at CIT-Alcatel, Paris, France. He is currently a professor of electrical engineering at University of Sétif, Algeria and Director of power electronics and industrial electronics laboratory. His main research interests are systems control, power and industrial electronics, renewable energies. In these fields, he has more than 100 papers in international journals and refereed conference proceedings. He is associate editor of IJECE journal and editorial member of four international journals. Professor Fateh Krim is a senior IEEE Member and member of IEEE Industrial Electronics Society, IEEE Power Electronics Society, IEEE Power Engineering Society IEEE Computational Intelligence Society. He was president of IEEE Algeria Section and Industrial electronics and Industry applications joint chapter. He can be contacted at email: krim_f_ieee_org@yahoo.fr, https://researcherid.com/rid/G-2151-2012

Abdelhamid Mansouri was born in Sidi-Okba, Algeria, in 1951. He received the D.E.S. (Diploma of High Studies) degree from the University of Algiers, in 1979 and the M.Phil. Degree in Electrical Engineering from the University of Setif in 1996. He was an assistant lecturer in the Department of Physics, University of Annaba in 1979. He was Electrical Engineer in Industrial Societies Enageo and Elatex from 1981 to 1983. Currently, he is a Lecturer in the Department of Electrical Engineering, University of Sétif, where he has been since 1983. Member of laboratory of power electronics and industrial control (LEPCI), his research interests are in the area of identification and optimal control of electrical machines and artificial intelligence techniques and renewable energies. He can be contacted at email: mansouri51@yahoo.com.